

Insight into Disulfide Bond Catalysis in *Chlamydia* from the Structure and Function of DsbH, a Novel Oxidoreductase^{*[S]}

Received for publication, September 19, 2007, and in revised form, November 5, 2007. Published, JBC Papers in Press, November 14, 2007, DOI 10.1074/jbc.M707863200

Thien-Thi Mac[‡], Annekathrin von Hacht[§], Kuo-Chan Hung[‡], Rachel J. Dutton^{¶1}, Dana Boyd^{¶1}, James C. A. Bardwell^{§2}, and Tobias S. Ulmer^{‡3}

From the [‡]Department of Biochemistry and Molecular Biology and Zilkha Neurogenetic Institute, Keck School of Medicine, University of Southern California, Los Angeles, California 90033, [§]Howard Hughes Medical Institute and Department of Molecular, Cellular, and Developmental Biology, University of Michigan, Ann Arbor, Michigan 48109, and [¶]Department of Microbiology and Molecular Genetics, Harvard Medical School, Boston, Massachusetts 02115

The *Chlamydia* family of human pathogens uses outer envelope proteins that are highly cross-linked by disulfide bonds but nevertheless keeps an unusually high number of unpaired cysteines in its secreted proteins. To gain insight into chlamydial disulfide bond catalysis, the structure, function, and substrate interaction of a novel periplasmic oxidoreductase, termed DsbH, were determined. The structure of DsbH, its redox potential of -269 mV, and its functional properties are similar to thioredoxin and the C-terminal domain of DsbD, *i.e.* characteristic of a disulfide reductase. As compared with these proteins, the two central residues of the DsbH catalytic motif (CMWC) shield the catalytic disulfide bond and are selectively perturbed by a peptide ligand. This shows that these oxidoreductase family characteristic residues are not only important in determining the redox potential of the catalytic disulfide bond but also in influencing substrate interactions. For DsbH, three functional roles are conceivable; that is, reducing intermolecular disulfides between proteins and small molecules, keeping a specific subset of exported proteins reduced, or maintaining the periplasm of *Chlamydia* in a generally reducing state.

Chlamydia are obligate intracellular eubacteria that are phylogenetically distant from other bacterial divisions (1). Virtually every human being will be infected with *Chlamydia pneumoniae* in their lifetime, and this organism accounts for $\sim 10\%$ of pneumonia cases and 5% of bronchitis cases in the United States (2, 3). Acute infections are usually mild in immunocompetent hosts, but severe pneumonias are observed in immunocompromised patients. Chronic *C. pneumoniae* infections have been associated with arterial disease (4), where *C. pneumoniae*

act to continuously stimulate inflammation and thereby contribute to stroke and coronary heart disease. *Chlamydia* have a unique developmental cycle in which the extracellular infectious form, the elementary body, is metabolically inactive and highly resistant to lysis. This is thought to be due in large part to a complex of outer envelope proteins that are highly cross-linked by disulfide bonds (5). Disulfide cross-linked envelope proteins appear to substitute for peptidoglycan in the elementary body (6). This is in contrast to the intracellular, non-infectious but metabolically active reticulate body which employs peptidoglycan (7), like other Gram-negative bacteria. The reliance of the elementary body on disulfide bond-linked proteins suggests that interference with chlamydial disulfide bond catalysis offers a potential avenue for treating chlamydial infections in addition to antibiotics administration. Despite the extensive use of disulfide cross-linked envelope proteins, *Chlamydia* exhibit an unusually high number of unpaired cysteines in their secreted proteins compared with *Escherichia coli*. Is the machinery for periplasmic disulfide bond catalysis in *Chlamydia* different from *E. coli*?

Functional gene assignment of the *C. pneumoniae* TW183 genome predicts 5 periplasmic oxidoreductases (8) of a total of 1113 predicted proteins. In comparison, *E. coli* K-12, for which the catalysis of periplasmic disulfide bond formation has been characterized best (9, 10), possesses 6 periplasmic oxidoreductases of a total of 4243 predicted proteins. The five central disulfide bond-forming proteins (Dsb)⁴ of *E. coli* catalyze the *de novo* formation of disulfide bonds as well as the isomerization of incorrectly formed disulfide bonds to the correct form. DsbB and DsbA form the functional pair that acts, respectively, to create disulfide bonds and transfer them to substrate proteins. The lack of DsbA, which is the primary periplasmic dithiol oxidant, greatly reduces the virulence of several bacterial species (11, 12), providing further evidence for the potential of treating chronic *Chlamydia* infections by interfering with disulfide bond catalysis. Reduced DsbA is reoxidized by the integral inner membrane protein DsbB (13, 14), which in turn regenerates its disulfide bonds by reducing ubiquinone within the membrane (15, 16). Disulfide bond isomerization is thought to be catalyzed by the DsbC-DsbD and DsbG-DsbD pairs. The

* The costs of publication of this article were defrayed in part by the payment of page charges. This article must therefore be hereby marked "advertisement" in accordance with 18 U.S.C. Section 1734 solely to indicate this fact.

[S] The on-line version of this article (available at <http://www.jbc.org>) contains supplemental Figs. 1–3 and Tables 1–4.

The atomic coordinates and structure factors (code 2ju5) have been deposited in the Protein Data Bank, Research Collaboratory for Structural Bioinformatics, Rutgers University, New Brunswick, NJ (<http://www.rcsb.org/>).

¹ Supported by National Institutes of Health Grant GMO41883 (to J. Beckwith).

² Supported by grants from the National Institutes of Health and is an Investigator of the Howard Hughes Medical Institute.

³ To whom correspondence should be addressed: 1501 San Pablo St, ZNI 111, Los Angeles, CA 90033. Tel.: 323-442-4326; Fax: 323-442-2145; E-mail: tulmer@usc.edu.

⁴ The abbreviations used are: Dsb, disulfide bond-forming protein; BLAST, basic local alignment search tool; HPLC, high performance liquid chromatography; NOE, nuclear Overhauser effect.

soluble DsbC and DsbG proteins are kept in their active reduced state by the transmembrane protein DsbD (17, 18). In turn, DsbD gains its reducing equivalents from the cytosolic protein thioredoxin, which ultimately gains its reduced equivalents from NADPH (18). DsbE(CcmG), which is also kept reduced by the DsbD protein, is required for cytochrome *c* maturation. DsbE is thought to be responsible for keeping two cysteine residues in cytochromes reduced, a prerequisite for heme attachment (19).

The present study identifies two new subfamilies of periplasmic oxidoreductases in *Chlamydia*, termed DsbH and DsbJ, besides orthologs of DsbA, DsbB, and DsbD. As a first step in the characterization of the chlamydial disulfide bond catalysis, the solution structure of DsbH was determined to establish its structural relationship to the known oxidoreductases. To learn more about DsbH-substrate interactions, the interaction of DsbH with a peptide ligand was examined. The functional characterization of DsbH enzymatic properties was carried out, and the results suggest that DsbH plays the role of a reducing thiol disulfide oxidoreductase in *Chlamydia*. Compared with for example *E. coli*, the disulfide bond catalysis machinery of *Chlamydia* exhibits substantial differences.

EXPERIMENTAL PROCEDURES

Molecular Biology—The DsbH gene of *C. pneumoniae* TW-183 (CpB0958) was assembled from overlapping oligonucleotides (Retrogen, Inc.). A C41G substitution was implemented based on sequence alignment with *Chlamydia caviae* GPIC (data not shown). For efficient periplasmic expression in *E. coli*, the DsbA signal sequence from *E. coli* was used instead of that from DsbH. A high sequence homology between the two signal sequences and the unambiguously predicted DsbH signal peptide cleavage site using the program SignalP 3.0 (20) (supplemental Fig. 1) form a sound rationale for this approach. The DsbH gene was cloned into the pET-44 vector (Novagen, Inc.) for expression in conjunction with a C-terminal His₆ tag. For *in vivo* functional assays, another periplasmic expression vector (pET44-DsbH) was prepared that is devoid of a His₆ tag. A third expression construct in which the His₆ tag is shifted to the N terminus and replaces the signal sequence was also constructed for cytosolic protein localization. The DNA of the peptide ligand encompassing two disulfide bond motifs (Fig. 5D) and a preceding tobacco etch virus protease cleavage site was synthesized from overlapping oligonucleotides and ligated into pET-44 as a fusion to the third IgG binding domain (GB3).

Protein Biochemistry—Periplasmic DsbH expression was induced in *E. coli* BL21(DE3) cells growing in M9 minimal media at 20 °C at an A_{600} of 0.6 by adding isopropyl 1-thio- β -D-galactopyranoside to 0.5 mM. After overnight expression, the cells were harvested by centrifugation and lysed by sonication in ice-cold 50 mM Tris-HCl, pH 8.0, 300 mM NaCl, 10 mM imidazole solution. The clarified lysate was applied on a HiTrap Chelating HP column (GE Healthcare) charged with Ni²⁺ for immobilized metal affinity chromatography. Bound proteins were eluted using a two-step gradient (50 and 300 mM imidazole). Subsequently, DsbH was purified to homogeneity by gel filtration chromatography using a Sephacryl S100 column (GE Healthcare) in 25 mM NaH₂PO₄/Na₂HPO₄, pH 6.5, 150 mM

NaCl buffer. The cytosolic DsbH expression vector was used in *E. coli* BL21Star(DE3) cells (Stratagene, Inc.), and DsbH expression was induced at A_{600} = 0.8 for 4 h at 37 °C. Cells were lysed in 50 mM Tris-HCl pH 8.0, 300 mM NaCl, 10 mM imidazole, 8 M urea, 2 mM β -mercaptoethanol solution, and the cleared lysate was again applied on the immobilized metal affinity chromatography column. After extensive washing in lysis buffer, urea was eliminated from the wash buffer, and subsequently, β -mercaptoethanol was also eliminated, allowing protein folding and disulfide bond formation before protein elution. The remainder of the purification was identical to that for periplasmic DsbH. The GB3-peptide construct was expressed and purified analogously to cytosolic DsbH. The monomeric GB3-peptide fraction from gel filtration containing only intramolecular disulfide bonds was cleaved with tobacco etch virus protease in the absence of any reducing agents at a molar ratio of 1:200 overnight at room temperature. Fusion protein and tobacco etch virus protease were removed from the peptide by immobilized metal affinity chromatography.

NMR Sample Preparation—Samples of 300- μ l volumes were prepared in 50 mM NaH₂PO₄/Na₂HPO₄, pH 6.0, and 0.02% w/v NaN₃ buffer to contain 1.0 mM of DsbH (cytosolic; $\epsilon_{280\text{ nm}}$ = 21,030 M⁻¹cm⁻¹). Besides a sample in isotropic solution, the alignment of DsbH relative to the magnetic field was achieved in the presence of bicelles and stretched polyacrylamide gel. A 5% solution of bicelles consisting of 1,2-di-*O*-tridecanyl-*sn*-glycero-3-phosphocholine (DTPC), 1,2-di-*O*-hexyl-*sn*-glycero-3-phosphocholine (DHPC), and cetyltrimethylammonium bromide (CTAB) at molar ratios of DTPC:DHPC = 3:1 and (DTPC+DHPC):CTAB = 30:1 was employed. Stretched, negatively charged polyacrylamide gels (21) were polymerized from a 5.1% w/v solution of acrylamide, 2-acrylamido-2-methyl-1-propanesulfonate (AMPS), and bisacrylamide with a monomer to cross-linker ratio of 39:1 (w/w) and a molar ratio of 98:2 of acrylamide to AMPS, employing the previously described conventions and procedures (22). The bicelle solution gave rise to a ²H splitting of 22.8 Hz at 29 °C, corresponding to a DsbH alignment tensor magnitude of 10.4 Hz. For the stretched gel a ²H splitting of 2.4 Hz was detected at 25 °C, corresponding to a tensor magnitude of 10.1 Hz. DsbH samples containing the employed peptide ligand (Fig. 5D) were prepared to contain 0.1 mM ¹⁵N-labeled DsbH and 0.05 mM peptide in the above phosphate buffer.

NMR Spectroscopy—All experiments were carried out on a Bruker Avance 700 spectrometer at 25 °C except for the bicelle solution, which was measured at 29 °C to maintain the liquid crystalline phase. Data were processed and analyzed with the nmrPipe package and CARA. H^N, N, C ^{α} , C ^{β} , and C' assignments were made from HNCA, HNCACB, HNCO, and CBCA(CO)NH experiments. Subsequently, H ^{α} and partial H ^{β} assignments were obtained from total correlation spectroscopy-heteronuclear single quantum correlation experiments (t_{mix} = 35.9 ms). The side-chain assignments were completed using H(C)CH-*J*-correlation spectroscopy (COSY) and (H)CCH-COSY experiments (23). Partial assignments of the highly overlapped aromatic side chains were obtained from their constant time (CT)-heteronuclear single quantum correlation and NOE spectroscopy pat-

terns (24). ^{15}N - and ^{13}C -edited NOE spectroscopy spectra were recorded with a mixing time of 100 ms. NOE cross-peak assignments were performed manually. $^3J_{\text{C}'\text{C}\gamma}$ and $^3J_{\text{NC}\gamma}$ couplings for aromatic and aliphatic residues were obtained from quantitative J -correlation spectroscopy (25) with dephasing times of 50 and 100 ms, respectively. $^1J_{\text{NH}}$, $^1J_{\text{C}\alpha\text{C}'}$, $^1J_{\text{C}'\text{N}}$ and $^1J_{\text{NH}} + ^1D_{\text{NH}}$, $^1J_{\text{C}\alpha\text{C}'} + ^1D_{\text{C}\alpha\text{C}'}$, $^1J_{\text{C}'\text{N}} + ^1D_{\text{C}'\text{N}}$ couplings were determined from mixed-constant time, H^{N} -coupled HNCO (26), and quantitative J -correlation HNCO experiments (27, 28) of isotropic and aligned samples, respectively. $\{\text{H}\}$ - ^{15}N NOE measurements were carried out at 70.9 MHz (29) using 3 s of presaturation preceded by a recycling delay of 2 s for the NOE experiment and a 5-s recycle delay for the reference experiment.

Structure Calculation— ϕ , θ backbone dihedral angle restraints were extracted from H^α , N, C^α , C^β , and C' chemical shifts using the program TALOS (30). χ_1 side-chain angle restraints were derived from the $^3J_{\text{C}'\text{C}\gamma}$ and $^3J_{\text{NC}\gamma}$ coupling constants (25). Proline *cis/trans* assignments were based on the proline ^{13}C chemical shift pattern (31). NOE peak amplitudes were converted into interproton distances using an empirical $1/r^4$ correlation between amplitude and distance (32). Distances were calibrated in α -helical regions by matching interproton $\text{dN}_i\text{N}_{i+1}$ and $\text{dN}_i\text{N}_{i+3}$ distances for ^{15}N -edited and interproton $\text{d}\alpha_i\text{N}_{i+1}$ and $\text{d}\alpha_i\text{N}_{i+2}$ distances for ^{13}C -edited NOE spectroscopy spectra to values found in α -helical conformation. The distance restraints were grouped into four ranges, 1.8–2.7 Å (1.8–2.9 Å for NOEs involving H^{N} protons), 1.8–3.3 Å (1.8–3.5 Å for NOEs involving H^{N} protons), 1.8–5.0 Å, and 1.8–6.0 Å, corresponding to strong, medium, weak, and very weak NOEs, respectively. To account for the higher apparent intensity of methyl resonances, the upper distance bound for NOEs involving methyl groups was extended by 0.5 Å. Interproton distances involving non-stereospecifically assigned methylene protons, methyl groups, and H δ and He protons of Tyr and Phe were represented as a $(\sum r^{-6})^{-1/6}$ sum (33). The alignment tensor magnitude and rhombicity for each residual dipolar coupling data set were estimated from molecular fragment replacement (34) and were kept fixed during structure calculations. Alignment tensor magnitudes of 10.4 and 10.1 Hz were obtained for the employed bicelle and gel media, respectively, eliminating the need for media-specific weighting factors.

DsbH structures were calculated by simulated annealing starting at 3000 K using the program XPLOR-NIH (35). Besides standard force field terms for covalent geometry (bonds, angles, and improper torsions) and nonbonded contacts (van der Waals repulsion), the following experimental and empirical potentials were included. Dihedral angle restraints and interproton distance restraints were implemented using quadratic square-well potentials. The difference between predicted and experimental residual dipolar couplings was described by a quadratic harmonic potential. A pseudopotential for the radius of gyration was used (36) as well as a backbone-backbone hydrogen-bonding potential (37) and torsion angle potentials of mean force (38). An ensemble of 20 structures was calculated. The structural statistics are summarized in supplemental Table 1. Atomic coordinates, structural restraints and chemical shift assignments for DsbH have been deposited in the Protein

Data Bank and Biological Magnetic Resonance Bank under ID codes 2ju5 and 15431, respectively.

Redox Potential Measurement—Proteins whose redox potentials were to be measured were incubated with DsbD γ , a protein of known redox potential, -235 mV (39). At equilibrium different protein species were separated by reverse-phase HPLC, and the equilibrium constant (K_{eq}) of the reaction and the standard redox potential (E°) of the protein were determined as described (40). To verify that equilibrium was reached, it was approached from both directions. To do this DsbD γ was incubated separately with the reduced and the oxidized forms of the protein. Values obtained from these parallel experiments were within 1 mV of each other, showing that equilibrium had been closely approached. A value of -240 mV was used for the standard redox potential of glutathione at pH 7.0 to calculate the standard redox potential of DsbH (41).

Insulin Turbidity Assay—The ability of DsbH to catalyze the reduction of bovine insulin was tested using an insulin turbidity assay. The reaction mixture, containing 131 μM insulin, 0.35 mM dithiothreitol, and 1, 5, or 8 μM reduced protein (thioredoxin and DsbH) and the insulin stock were prepared in 0.1 M potassium phosphate buffer, pH 7, 2 mM EDTA. The final volume was 1 ml, and the reaction was started by adding insulin. The measurements were performed at 650 nm. The uncatalyzed reduction of insulin by dithiothreitol was monitored in a control reaction without adding reduced protein.

Measurement of Oxidase Activity by Stopped Flow—Stopped flow fluorescence measurements were performed on a KinTek SF-2004 instrument in single-mixing mode. The typical reaction contained 0.5 μM oxidized protein (DsbA, thioredoxin, DsbH) and 2.5, 5, 7.5, and 10 μM reduced hirudin, respectively. The oxidized proteins and reduced hirudin were incubated in 100 mM sodium phosphate buffer containing 1 mM EDTA, pH 7.0, at 25 °C before mixing. An excitation wavelength of 295 nm and a bandpass filter were used to monitor the fluorescence change of the proteins.

Isomerization of Scrambled Hirudin—21 μM scrambled hirudin and 21 μM freshly reduced protein (DsbH, *E. coli* DsbC, and thioredoxin) were incubated in 20 mM sodium phosphate, 130 mM sodium chloride, 0.13% polyethylene glycol 8000 at 25 °C. Aliquots of 120 μl were removed after different reaction times and quenched with 15 μl of formic acid and 15 μl of acetonitrile. Hirudin folding intermediates were separated by reverse-phase HPLC on a C18 column at 55 °C in a 19–25% acetonitrile gradient in 0.1% (v/v) trifluoroacetic acid. The absorbance was recorded at 220 nm.

Spot Titers for Cadmium and Copper Resistance—Spot titers for cadmium resistance were performed to assay the ability of DsbH to complement DsbA. For this assay, the strain JP120 (supplemental Table 2) was transformed with the periplasmic DsbH expression vector (pET44-DsbH) by electroporation. Briefly, mid-log phase cells ($A_{600} \approx 1$) were serially diluted in sterile 170 mM NaCl solution. 2 μl of each dilution was plated onto LB plates supplemented with CdCl_2 in a concentration of 5, 6, and 7.5 μM . After 16 h at 37 °C, the growth of each strain at different cadmium concentrations was compared, and the cad-

TABLE 1

C. pneumoniae oxidoreductase functional gene assignments

Locus tag ^a	CpB0685	CpB0234	CpB0233	CpB0814	CpB0958	CpB0968
GenBank™ accession no.	NP_876957	NP_876510	NP_876509	NP_877086	NP_877230	NP_877239
Length	102	233	137	714	166	348
Assignment	Thioredoxin	DsbA	DsbB	DsbD	DsbH	DsbJ
PSI-Blast E-value to <i>E. coli</i> orthologue (third iteration)	3×10^{-43}	4×10^{-12}	2×10^{-11}	6×10^{-70}	No clear orthologue detected	No clear orthologue detected

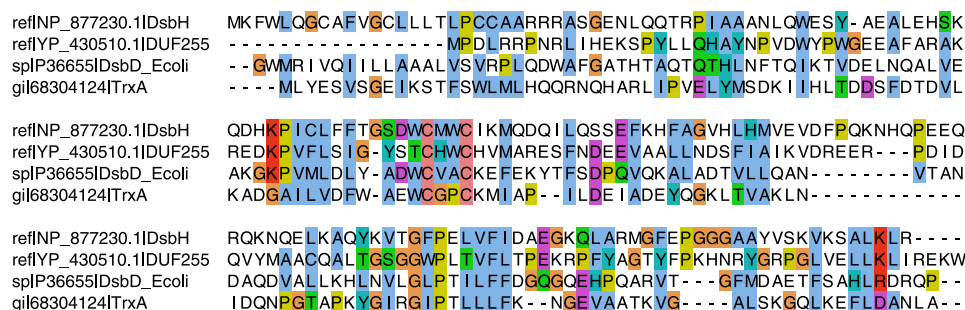
^a Locus tag refers to strain TW-183 of *C. pneumoniae*.

FIGURE 1. **DsbH sequence alignment.** ClustalW sequence alignment of DsbH from *C. pneumoniae* TW-183 and three other thioredoxin related proteins, including *E. coli* thioredoxin (*Trx*), the N terminus of a DUF255 family member (*DUF255*), and the C-terminal domain of *E. coli* DsbD (*DsbD*). Conserved amino acids are colored using the color scheme utilized by the Jalview multiple alignment editor (57).

mium resistance was ranked 1–7, with higher values indicating increased resistance (supplemental Table 3).

To assay the ability of DsbH to complement DsbC, the spot titers for copper resistance were made. The strains BW25113 and BW25113 *dsbC::kan* (supplemental Table 2) were transformed with the periplasmic DsbH expression vector (pET44-DsbH) by electroporation. As controls, the wild type strains and the untransformed strains were also spotted on the copper plates. Serial dilution was performed in a similar way as in cadmium resistance assays. 2 μ l of each dilution was plated onto brain heart infusion plates containing 5 mM CuCl₂ and on TB plates containing 15 mM CuCl₂. After incubation at 37 °C for 16 h, the growth of each strain was compared and ranked (Table 2).

Motility Assay—The motility assay was performed in M9 minimal soft agar plates (0.2%) supplemented with 18 amino acids (excluding cysteine and methionine), 0.4% glycerol, 2 μ g/ml nicotinamide, 0.2 μ g/ml riboflavin B2, 2 μ g/ml thiamine B1, 2 μ g/ml biotin, 1 mM MgSO₄ as described previously (42). Mid-log phase liquid cultures were diluted based on the absorbance at 600 nm to normalized cell density for 1 absorbance unit. 2 μ l of cells were then inoculated into the center of the motility plate. After 18 h of incubation at 37 °C, the diameter of the swarm was measured (supplemental Table 4).

RESULTS AND DISCUSSION

Functional Gene Assignment of Chlamydial Disulfide Oxidoreductases—The amino acid sequences of the five predicted periplasmic oxidoreductases of *Chlamydia* (8) were subjected to position-specific iterative BLAST searches to identify homologies to Dsb proteins. Chlamydial orthologs of DsbA, DsbC, and DsbD were identified this way (Table 1). However, the remaining two proteins, although distantly related to a number of thioredoxin family proteins, were not closely related to any described Dsb protein including DsbA, DsbB, DsbC, DsbD, DsbE, DsbG, or any other thioredoxin-related protein of known function. Thus, they appear to represent new subfam-

ilies of thioredoxin related proteins. Because the common function of thioredoxin-related proteins is thiol-disulfide exchange, the two proteins are termed DsbH and DsbJ, respectively (Table 1), to highlight their putative involvement in periplasmic disulfide bond manipulation. It is further noted that for both proteins signal peptides are predicted with very high probabilities of 0.987 and 0.999 using the program SignalP 3.0 (supplemental Fig. 1) (20), clearly indicating the

periplasmic localization of DsbH and DsbJ.

Significant similarities to DsbH can be detected using position-specific iterative BLAST searches for a wide variety of thioredoxin-related proteins, including DUF255 (a thioredoxin-related protein family of unknown function), the C-terminal domain of DsbD (DsbD_γ), and somewhat more distantly, to thioredoxin itself (Fig. 1). It is noted that the term DsbH has previously been used in GenBank™ for proteins found in *Pseudomonas* (e.g. YP_001171076) and *Chromobacter*, but these proteins are clearly DsbB homologues and, thus, do not represent a new Dsb protein family. To learn more about the new DsbH family of thioredoxin-related periplasmic oxidoreductases, DsbH from *C. pneumoniae* is structurally and functionally characterized.

DsbH Structure Determination—The solution structure of oxidized DsbH was determined by multidimensional heteronuclear NMR spectroscopy, making use of uniformly ¹³C, ¹⁵N-labeled protein. As reflected by its rotational correlation time of 10.0 ns and gel filtration profile (supplemental Fig. 2), DsbH is a monomer in solution. A wealth of local structural information on interproton distances and dihedral angles was provided by NMR observables such as NOEs, coupling constants, and chemical shifts. In addition, an extensive set of residual dipolar couplings was used to improve the spatial relationship of more remote protein segments by relating the respective internuclear bond vector orientations to a common molecular alignment frame. The final ensemble of structures was calculated by simulated annealing on the basis of a total of 3410 experimental NMR restraints. Fig. 2A shows a superposition of the final ensemble of 20 simulated annealing structures for which a coordinate precision of 0.69 Å was obtained for all heavy atoms (in the well-folded DsbH domain). A summary of the structural statistics is provided in supplemental Table 1.

Description of the Structure—In accordance with its putative disulfide oxidoreductase role, residues Gln-20–Arg-144 of

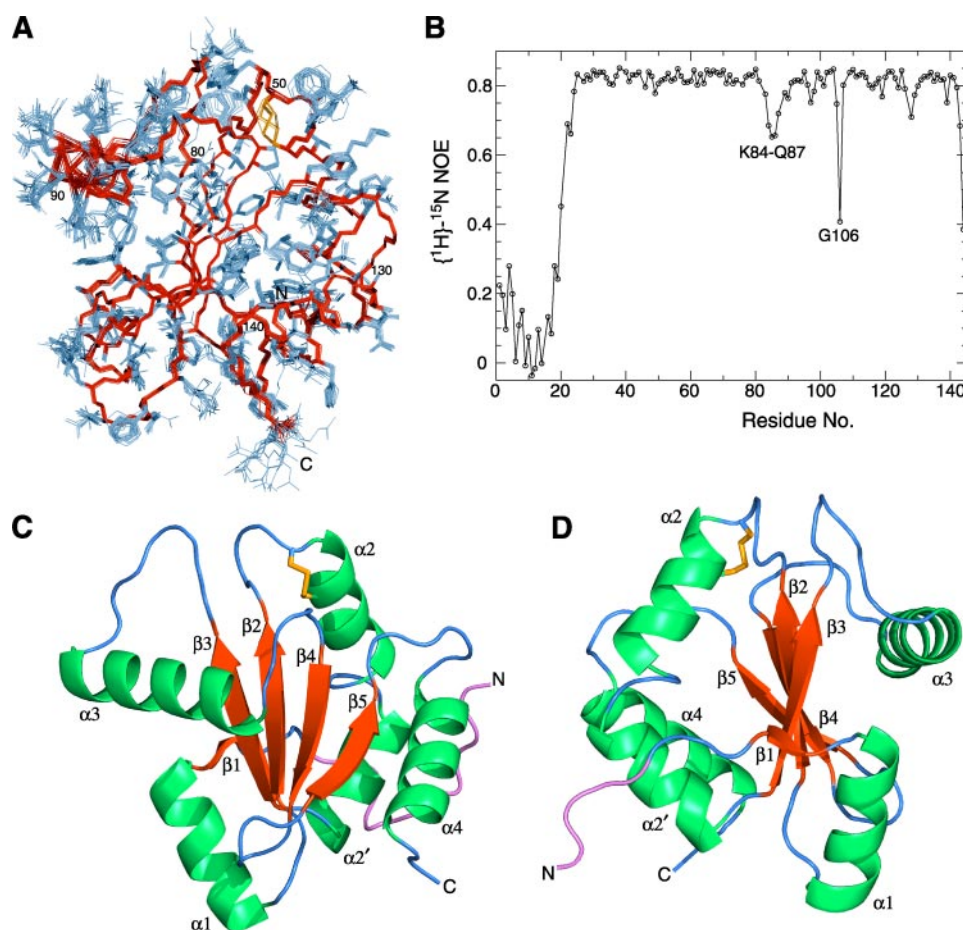


FIGURE 2. Solution structure of oxidized DsbH. A, superposition of the ensemble of 20 calculated simulated annealing structures. The unfolded N-terminal stretch, consisting of Ala-1—Ala-19, is omitted for clarity. The backbone is shown in red, the disulfide bridge (Cys-50—Cys-53) in yellow, and all other side chains in blue. B, fast timescale DsbH backbone dynamics. The heteronuclear $\{^1\text{H}\}$ - ^{15}N NOE, which is sensitive to backbone N-H bond vector fluctuations on the pico- to nanosecond timescale, establishes the unfolded nature of the first 19 residues. Residues Lys-84—Asn-87 and Gly-106 also show enhanced backbone dynamics. C and D, schematic representations of the DsbH structure. Loop regions are shown in blue, α -helices are shown in green, β -strands are in red, and the catalytic disulfide bridge (Cys-50—Cys-53) is in yellow. The end of the unfolded Ala-1—Ala-19 stretch is shown in violet.

DsbH adopt a thioredoxin fold (Fig. 2, C and D). Residues Ala-1 to Ala-19, which follow the predicted signal peptide cleavage site, are unfolded (Fig. 2B). Overall, five α -helices surround five central β -strands in the DsbH domain. The first β -strand (β 1) is almost perpendicular to the other β -sheets and consists of only two residues, Trp-23—Glu-24 (Fig. 2D); however, Leu-21—Asn-22 are also in extended conformations, and Leu-21 is intimately connected to the hydrophobic protein interior as shown by methyl-methyl NOEs to Leu-61 of the α 2- α 2' helix connector and Met-76 of strand β 3. The active site disulfide bond, Cys-50—Cys-53, is located at the beginning of helix α 2, which is typical for thioredoxin-like oxidoreductases (43). Likewise, the orientation of the longest helix, α 3, is striking in the sense that it is close to perpendicular to the central β -sheet as well as all other α -helices. β -Sheets β 2 to β 4 are moderately twisted relative to one another, but the β 4- β 5 pair shows a conspicuous twist (Fig. 2D). Strand β 5, comprising Gln-119—Met-123, runs along the α 4 helix axis accompanied by mainly hydrophobic side-chain contacts, as evidenced by, for example, methyl-methyl NOEs between Met-123 and Val-137 and Ala-121 and Leu-141. The twist at the end of β 5 leads to somewhat

suboptimal hydrogen bond geometries for the four interstrand hydrogen bonds between Leu-110 and Met-123 and Phe-112 and Ala-121. The intervening Arg-122 is fully solvent-exposed with the availability of water molecules as hydrogen-bond partners. Backbone dynamics on a fast timescale (pico- to nanosecond), which is indicative of secondary structure stability, identifies distinctive dynamics for the unfolded first 19 residues (as expected) and slightly elevated dynamics for Lys-84—Gln-87 and Gly-106 (Fig. 2B). These residues lie in the α 3- β 3 and α 3- β 4 connectors, respectively.

Similarities to Other Oxidoreductases—When comparing the structure of DsbH to other structures in the Protein Data Bank code, DsbH is most similar to the thioredoxin domain present in the C-terminal domain of DsbD (DsbD γ ; Z-score = 12.9). Structurally, DsbH is also highly similar to thioredoxin itself (Z-score = 11.2 for *E. coli* thioredoxin). In fact, the topology of DsbH is identical to thioredoxin, whereas DsbD γ contains an additional helix in exchange for strand β 5 (Fig. 3). Interestingly, unlike in thioredoxin, strand β 5 of DsbH is not well connected to its central β -sheet, as discussed above. The change in strand β 5 may, therefore, represent a meaningful evolutionary change over the original thioredoxin conformation. The higher structural similarity of DsbH to DsbD γ arises from the orientation and length of the α -helices in DsbH, which is a second notable change of both proteins compared with thioredoxin (Fig. 3, B and C). The increase in length from *E. coli* thioredoxin (109 residues) to the (folded) DsbH domain (125 residues) has been mainly incorporated into the α -helices, which now have a minimum of three turns. The “break” of the kinked thioredoxin helix α 2 into two shorter helices, α 2 and α 2', in DsbH and DsbD γ is also noteworthy (Fig. 3B). It allows helix α 2' to change its orientation relative to the central β -sheet and allows helix α 2 to adopt a longer linear segment (44).

The high structural homology between DsbH, DsbD γ , and thioredoxin exists despite the fact that the DsbH-thioredoxin and DsbH-DsbD γ pairs only share sequence identities of 18.9 and 16.5%, respectively. The levels of structural and sequence identity between DsbH, DsbD γ , and thioredoxin are similar to that found between DsbA and thioredoxin but much lower than the 43.5% sequence identity found between *E. coli* thioredoxin and its chlamydial orthologue (Table 1). Thus, although DsbH, DsbD γ , and thioredoxin are clearly structurally related, they are

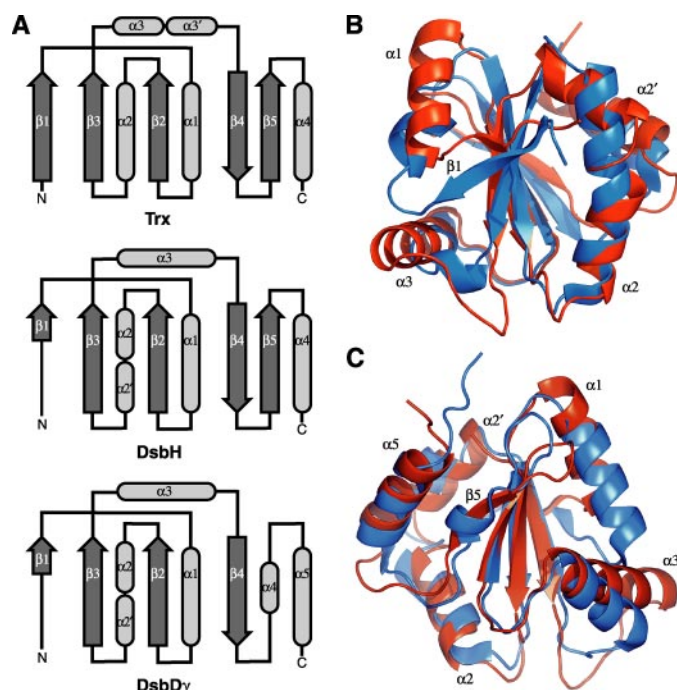


FIGURE 3. Comparison of DsbH topology and structure with thioredoxin and DsbDγ. A, thioredoxin (Trx) and DsbH exhibit identical topologies, whereas DsbDγ possesses an additional helix in exchange for strand β5. B, superposition of DsbH (red) with *E. coli* thioredoxin (blue; Protein Data Bank code 2TRX, chain A). 101 residues overlay with a backbone coordinate root mean square deviation of 2.3 Å (Z-score = 11.2). C, superposition of DsbH (red) with *E. coli* DsbDγ (blue; Protein Data Bank code 2FWE). 111 residues overlay with a backbone coordinate root mean square deviation of 2.5 Å (Z-score = 12.9).

at best distant homologues. *Chlamydia* does possess a full-length DsbD orthologue (Table 1), so DsbH is not orthologous to DsbD. In addition, DsbH lacks the membrane-embedded β domain and the periplasmic α domain found in DsbD. Thus, it is unlikely to perform the function of DsbD, namely, the transduction of reducing equivalents from the cytoplasm-located thioredoxin to a periplasmic thioredoxin-related protein such as DsbC. Rather, DsbH similarity to DsbDγ may reflect the evolutionary origin of DsbH. DsbDγ may have provided a convenient evolutionary progenitor for DsbH. The close structural similarity of DsbH, DsbDγ, and thioredoxin does not necessarily imply their functional similarity since the redox potential is critically dependent on the two central residues of the CXXC motif (45), which differ substantially among the three proteins (Fig. 1).

Functional Characterization of DsbH—To learn more about the functional characteristics of DsbH, its redox potential was measured, and its catalytic properties were compared with the oxidase DsbA, the reductase thioredoxin, and the isomerase DsbC. Despite the clear difference in catalytic motifs between DsbH (CMWC) and thioredoxin (CGPC), DsbH exhibits a redox potential of -269.7 ± 0.8 mV, which is virtually identical to thioredoxin, at -270 mV (46). DsbH is also indistinguishable from thioredoxin in its ability to reduce insulin *in vitro* (Fig. 4A), suggesting that DsbH, like thioredoxin, functions as a reducing thiol disulfide oxidoreductase *in vivo*. To test for the ability of DsbH to function as an oxidizing thiol-disulfide oxidoreductase, the rate of hirudin oxidation by DsbH was measured,

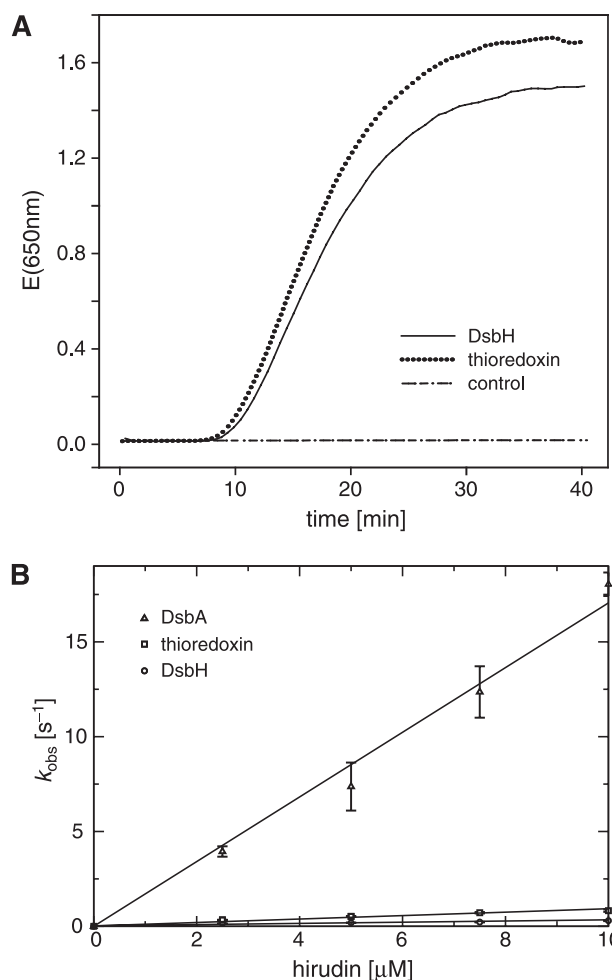


FIGURE 4. DsbH functional assays. A, insulin reduction assay. Measurement was performed two times, and the resulting data were averaged. Reduced proteins at concentrations of $5 \mu\text{M}$ were employed. B, kinetics of the oxidation of reduced hirudin by DsbA, thioredoxin, and DsbH. The second-order rate constants k_2 ($\text{M}^{-1}\text{s}^{-1}$) for the interaction of reduced hirudin and thioredoxin or DsbH are obtained by fitting the observed pseudo first-order rate constants k_{obs} (s^{-1}) against hirudin concentrations (M). The slopes are the apparent second-order rate constants for the reaction, and the values are $2 \times 10^6 \text{ M}^{-1}\text{s}^{-1}$ for DsbA, $80,947 \text{ M}^{-1}\text{s}^{-1}$ for thioredoxin, and $26,708 \text{ M}^{-1}\text{s}^{-1}$ for DsbH.

and its ability to complement the disulfide oxidase DsbA for motility and cadmium resistance was evaluated. DsbH is essentially unable to oxidize hirudin in comparison to DsbA (Fig. 4B) and fails to complement DsbA in cadmium resistance and motility assays (supplemental Tables 2–4). The isomerase activity of DsbH was tested by measuring its ability to isomerize the disulfides in misoxidized hirudin. The activity of DsbH in this assay was identical to the very weak isomerase activity exhibited by thioredoxin (data not shown), which is much weaker than the activity of the known isomerase DsbC (42). In addition, DsbH was unable to complement for DsbC in copper resistance assays (Table 2), showing the absence of isomerase functionality also *in vivo*. In addition, dimerization is known to be very important for disulfide isomerase activity (47, 48), but DsbH is a monomer in solution. Thus, in accordance with its redox potential, DsbH appears to be a periplasmic reductase. Before discussing possible functional roles of DsbH in *Chlamydia*, its active site characteristics are compared with the related

reductases thioredoxin and DsbD γ followed by the evaluation of a DsbH-peptide ligand interaction.

DsbH Active Site Characteristics—The catalytic disulfide bond of DsbH is surrounded by six key residues: Tyr-49, Met-51, Trp-52, Ile-54, Phe-107, and Pro-108 (Fig. 5, A and B). The functional relevance of some of these residues is reflected by rare conformations; Trp-49 exhibits a side-chain torsion angle, χ_1 , of $+48^\circ$ (Fig. 5, A and B), which makes it the only aromatic residue in DsbH with a χ_1 angle close to $+60^\circ$, and Pro-108 is in *cis* conformation. Moreover, the geometry of the catalytic Cys-

50—Cys-53 disulfide falls in the $+/-$ RHHook group, which classifies it as “catalytic,” like the disulfide of thioredoxin and DsbD γ (49). The active site backbone geometries of DsbH, DsbD γ , and thioredoxin are highly homologous (Fig. 5, A and B, and supplemental Fig. 3) and, therefore, allow a comparison of these key residues among the three proteins. The structurally homologous active site residues for DsbD γ are Trp-460, Val-462, Ala-463, Lys-465, Leu-510, and Pro-511, and for thioredoxin they are Trp-31, Gly-33, Pro-34, Lys-36, Ile-75, and Pro-76 (Fig. 5C). Again, both prolines are *cis* conformation, and χ_1 of Trp-460 and Trp-31 are $+36^\circ$ and $+41^\circ$, respectively, similar to Trp-49 of DsbH.

The largest difference among the active site residues is seen in the two central residues of the catalytic motifs, which reside on the solvent-exposed side of helix α_2 (Fig. 5, A and B). Compared with Met-51—Trp-52 of DsbH, Val-481—Ala-482 of DsbD γ as well as Gly-33—Pro-34 of thioredoxin are small and pose less steric hurdles upon approaching the catalytic disulfide (Fig. 5, A and B, and supplemental Fig. 3). In place of the charged Kys-484 and Lys-36 residues of DsbD γ and thioredoxin, the hydrophobic Ile-54 residue is inserted in DsbH (Fig.

5C), making its active site residues exclusively hydrophobic and bulky. Phe-107 of DsbH is also slightly more protective of the catalytic disulfide than Leu-510 and Ile-75 of DsbD γ and thioredoxin, respectively (Fig. 5, A and B, and supplemental Fig. 3). Taken together, it appears that the readily accessible active site disulfide of thioredoxin is most interested in productive substrate encounters, whereas substrate approach to DsbH is sterically more hindered and more geared toward hydrophobic substrates. DsbD γ appears intermediate between thioredoxin and DsbH. Finally, there is one more residue in the vicinity of the active site that is noteworthy; that is, Gly-106 of DsbH, which is also preserved in DsbD γ , thioredoxin, and even DUF255 (Figs. 5C and 1). In addition to being the smallest and conformationally most flexible residue, Gly-106 shows elevated backbone dynamics in DsbH (Fig. 2B). Conformational flexibility at Gly-106 may be of importance during catalysis when the catalytic disulfide engages a substrate and Phe-107 and Pro-108 may have to move out of the way (Fig. 5, A and B).

DsbH Interaction with a Peptide Ligand—The large nature of the prominent Met-51 and Trp-52 side chains of DsbH (Fig. 5, A and B) sug-

TABLE 2

Rank order copper resistance

Strain ^a	Rank order ^b
SQ416	2
SQ416 pET44-DsbH	2
SQ451	4
SQ451 pET44-DsbH	4
SQ417	6
SQ453	7

^a Strain descriptions are given in supplemental Table 2.

^b Copper resistance was ranked 1–7, with higher values indicating increased resistance.

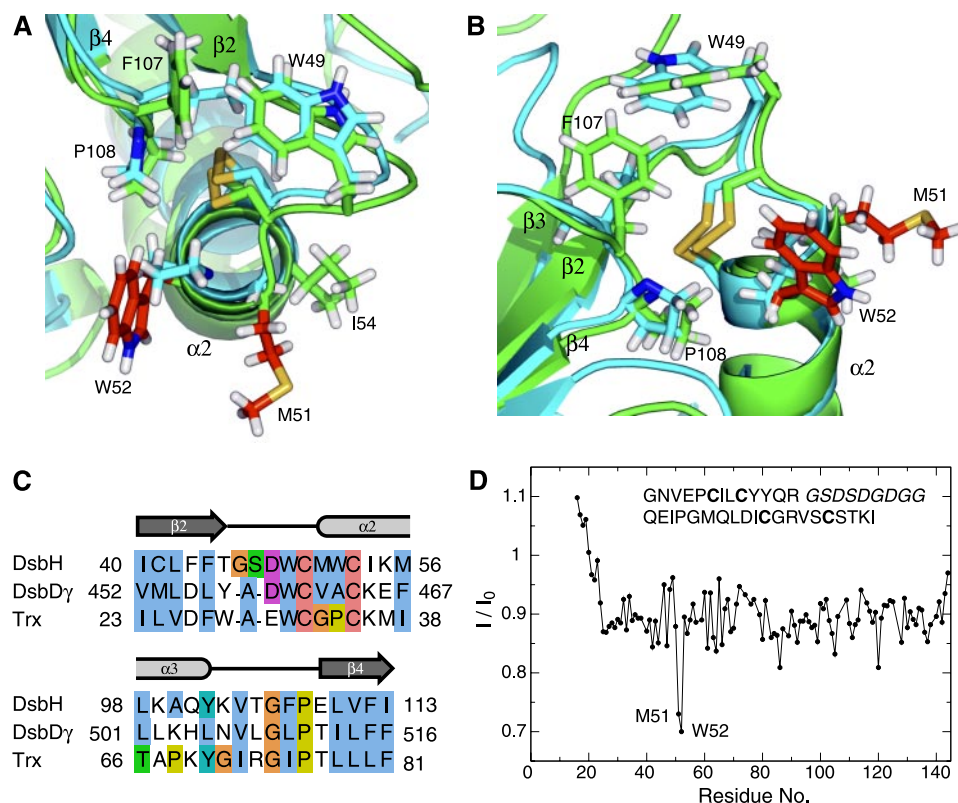


FIGURE 5. Comparison of DsbH and thioredoxin active site geometries and DsbH interaction with a peptide ligand. A and B, superposition of the active sites of DsbH (green) and *E. coli* thioredoxin (Trx; cyan; Protein Data Bank code 2TRX, chain A). Key amino acid residues are shown in ball-and-stick representation and are labeled for DsbH. Lys-36 of thioredoxin is omitted for clarity. C, sequence alignment of the active site residues. D, interaction of DsbH with the depicted peptide ligand encompassing two disulfide bond motifs. The DsbH backbone N-H heteronuclear single quantum coherence signal intensities, I/I_0 , in the absence and presence of the peptide is plotted as a function of residue number. Reproducible, selective broadening is observed for Met-51—Trp-52 (colored red in panels A and B) as a consequence of the DsbH-peptide interaction. In the fast DsbH-peptide exchange regime on the NMR timescale, the I/I_0 ratio is proportional to the square of the chemical shift differences (ω^2) between the free and bound DsbH state and the transverse relaxation rate of the bound state (R_{2B}). The unfolded DsbH residues (Ala-1—Ala-19), whose motions are uncoupled from the DsbH domain (Fig. 2B), exhibit incrementally higher I/I_0 ratios, most likely because of a change in their accessible conformational space and/or amide proton solvent exchange rates due to the vicinity of peptide. Specific, stable contacts with the peptide would result in lower I/I_0 ratios.

gests that any ligand approaching the catalytic disulfide would have to contact these two residues. A peptide that encompasses two disulfide bond motifs (Fig. 5D) was used to test this hypothesis. The peptide was not designed to specifically complement the DsbH active site, which is expected to reduce any (accessible) disulfide bond with reaction kinetics that are modulated by the specific disulfide bond environment of the ligand. Pursuant to our hypothesis, the peptide selectively perturbs the Met-51 and Trp-52 resonances of DsbH (Fig. 5D), demonstrating that these two residues are important for enzyme-substrate interactions. In the absence of an actual catalytic turnover, the interaction between the two oxidized partners is overall weak as judged from the modest effects on the NMR spectrum (Fig. 5D).

For thioredoxin, three structures of ligand-protein complexes are available (50–52). In all three cases the complexes are stabilized by an intermolecular disulfide bond and, therefore, represent a catalytic intermediate rather than the ligand approach to and departure from the active site observed here. Nevertheless, the structures suggest that the two rather small central residues of the thioredoxin catalytic motif, CGPC, do not substantially contribute to thioredoxin-substrate interactions. Thus, the central two residues of the dithiol oxidoreductase catalytic CXXC motif are not only crucial for determining the redox potential and reactivity of an oxidoreductase (45) but can also exert control over enzyme-substrate interactions, *i.e.* influence substrate selectivity and, thereby, reaction kinetics (Fig. 4). These two factors may explain the rich variety of these residues in the different oxidoreductase families (43, 52) of which each is adapted to its own set of substrates and regeneration partner.

Functional Role of DsbH in *Chlamydia*—Three functions appear conceivable for a periplasmic reductase in *Chlamydia*. DsbH may reduce mixed disulfides between proteins and small molecules in the periplasm. Another possible function is to keep a specific subset of periplasmic proteins in the reduced state. Third, DsbH may be responsible for keeping the thiol disulfide status of the periplasm generally reducing. Which of the three outlined scenarios is most probable?

Although the small molecule thiol content of the *C. pneumoniae* periplasm is unknown, a wide variety of thiol-containing compounds is present in the periplasm of *E. coli* (53). Recently, an ATP binding cassette-type transporter has been identified in *E. coli* that can mediate GSH and cysteine transport into the periplasm (54, 55). This means that, at least in the *E. coli* periplasm, there is the potential to form mixed disulfides with small molecules.

Cysteine residues can be involved in the ligation of a number of cofactors including hemes, iron sulfur clusters, and metal ions. To be functional in these ligation reactions, the cysteines need to be in the reduced form. Consequently, DsbH may be involved in the specific reduction of cysteine residues in cofactor-containing periplasmic proteins and membrane proteins with periplasmic domains. A reducing function of this type has already been suggested for the DsbE/TlpA/HelX family of inner membrane proteins (56). DsbH is only distantly related to DsbE/TlpA/HelX family members, and DsbH is also different from them in that it lacks a membrane-anchoring domain.

TABLE 3

Cysteine distribution in secreted proteins of *E. coli* and *C. pneumoniae* (comprising predicted transmembrane and secreted proteins)

The reported numbers are for *E. coli* strain K12 and *C. pneumoniae* strain TW-183. Other strains yield similar numbers.

	No. proteins (%) with an even number of cysteines	No. proteins (%) with an odd number of cysteines	Ratio even/odd
<i>E. coli</i>	720 (61%)	454 (39%)	1.58
<i>C. pneumoniae</i>	125 (43%)	167 (57%)	0.75

Finally, DsbH may be responsible for keeping a generally reducing periplasm. Such a scenario would be reflected in the ratio of even to odd cysteine residues for all chlamydial periplasmic proteins. This can be attributed to the tendency of unpaired cysteines to form incorrect disulfide bonds in an oxidizing milieu and the resulting expectation that, for example, *E. coli* with an oxidizing periplasm favors periplasmic proteins with even numbers of cysteines. *E. coli* has a ratio of even to odd numbers of cysteines of 1.58 (Table 3) fulfilling the expectation. In *Chlamydia*, however, there are more secreted proteins with an odd number of cysteines than an even number, resulting in an even to odd ratio of 0.75 (Table 3). This reversal of the balance of even to odd cysteines correlates with the emergence of DsbH in *C. pneumoniae* and suggests that *Chlamydia* do not oxidize periplasmic cysteines to disulfides. Instead, *Chlamydia* may keep their cysteine-containing periplasmic proteins in the reduced state.

It should be noted that *Chlamydia* do contain DsbA and DsbB orthologues (Table 1) that are expected to function to oxidize protein cysteines. However, these DsbAB homologues may function in a specialized role in oxidizing outer envelope cysteine rich periplasmic proteins to form a peptidoglycan equivalent. A generally reducing periplasm may benefit *Chlamydia* in their specific environment, which is intracellular. As an obligate organism, a reducing periplasm may represent an adaptation to the reducing cytosol of the host. In conclusion, although there is no direct evidence for the role of DsbH nor for why the periplasm of *Chlamydia* has a higher number of proteins with an even number of cysteines than many other bacteria, an attractive possibility is that DsbH might be responsible for maintaining a reducing periplasm.

Acknowledgments—We thank Jon Beckwith for communicating unpublished results. We are indebted to Charles Schwieters for scripts and helpful discussions regarding structural statistics.

REFERENCES

1. Pace, N. R. (1997) *Science* **276**, 734–740
2. Grayston, J. T. (2000) *J. Infect. Dis.* **181**, Suppl. s3, S402–S410
3. Kuo, C. C., Jackson, L. A., Campbell, L. A., and Grayston, J. T. (1995) *Clin. Microbiol. Rev.* **8**, 451–461
4. Sako, T., Takahashi, T., Takehana, K., Uchida, E., Nakade, T., Umemura, T., and Taniyama, H. (2002) *Atherosclerosis* **162**, 253–259
5. Everett, K. D. E., and Hatch, T. P. (1995) *J. Bacteriol.* **177**, 877–882
6. Hatch, T. P. (1996) *J. Bacteriol.* **178**, 1–5
7. McCoy, A. J., and Maurelli, A. T. (2006) *Trends Microbiol.* **14**, 70–77
8. Kalman, S., Mitchell, W., Marathe, R., Lammel, C., Fan, L., Hyman, R. W., Olinger, L., Grimwood, L., Davis, R. W., and Stephens, R. S. (1999) *Nat. Genet.* **21**, 385–389
9. Glockshuber, R. (1999) *Nature* **401**, 30–31

10. Inaba, K., Takahashi, Y., Ito, K., and Hayashi, S. (2006) *Proc. Natl. Acad. Sci. U. S. A.* **103**, 287–292
11. Yu, J., and Kroll, J. S. (1999) *Microbes Infect.* **1**, 1221–1228
12. Peek, J. A., and Taylor, R. K. (1992) *Proc. Natl. Acad. Sci. U. S. A.* **89**, 6210–6214
13. Missiakas, D., Georgopoulos, C., and Raina, S. (1993) *Proc. Natl. Acad. Sci. U. S. A.* **90**, 7084–7088
14. Bardwell, J. C. A., Lee, J. O., Jander, G., Martin, N., Belin, D., and Beckwith, J. (1993) *Proc. Natl. Acad. Sci. U. S. A.* **90**, 1038–1042
15. Bader, M., Muse, W., Ballou, D. P., Gassner, C., and Bardwell, J. C. A. (1999) *Cell* **98**, 217–227
16. Inaba, K., Murakami, S., Suzuki, M., Nakagawa, A., Yamashita, E., Okada, K., and Ito, K. (2006) *Cell* **127**, 789–801
17. Bessette, P. H., Cotto, J. J., Gilbert, H. F., and Georgiou, G. (1999) *J. Biol. Chem.* **274**, 7784–7792
18. Rietsch, A., Bessette, P., Georgiou, G., and Beckwith, J. (1997) *J. Bacteriol.* **179**, 6602–6608
19. Grove, J., Busby, S., and Cole, J. (1996) *Mol. Gen. Genet.* **252**, 332–341
20. Bendtsen, J. D., Nielsen, H., von Heijne, G., and Brunak, S. (2004) *J. Mol. Biol.* **340**, 783–795
21. Ulmer, T. S., Ramirez, B. E., Delaglio, F., and Bax, A. (2003) *J. Am. Chem. Soc.* **125**, 9179–9191
22. Ulmer, T. S., Bax, A., Cole, N. B., and Nussbaum, R. L. (2005) *J. Biol. Chem.* **280**, 9595–9603
23. Gehring, K., and Ekiel, I. (1998) *J. Magn. Reson.* **135**, 185–193
24. Lin, Z., Xu, Y. Q., Yang, S., and Yang, D. W. (2006) *Angew. Chem. Int. Ed. Engl.* **45**, 1960–1963
25. Hu, J. S., Grzesiek, S., and Bax, A. (1997) *J. Am. Chem. Soc.* **119**, 1803–1804
26. Cornilescu, G., and Bax, A. (2000) *J. Am. Chem. Soc.* **122**, 10143–10154
27. Jaroniec, C. P., Ulmer, T. S., and Bax, A. (2004) *J. Biomol. NMR* **30**, 181–194
28. Chou, J. J., Delaglio, F., and Bax, A. (2000) *J. Biomol. NMR* **18**, 101–105
29. Farrow, N. A., Muhandiram, R., Singer, A. U., Pascal, S. M., Kay, C. M., Gish, G., Shoelson, S. E., Pawson, T., Formankay, J. D., and Kay, L. E. (1994) *Biochemistry* **33**, 5984–6003
30. Cornilescu, G., Delaglio, F., and Bax, A. (1999) *J. Biomol. NMR* **13**, 289–302
31. Schubert, M., Labudde, D., Oschkinat, H., and Schmieder, P. (2002) *J. Biomol. NMR* **24**, 149–154
32. Guntert, P., Braun, W., and Wuthrich, K. (1991) *J. Mol. Biol.* **217**, 517–530
33. Nilges, M. (1993) *Proteins* **17**, 297–309
34. Delaglio, F., Kontaxis, G., and Bax, A. (2000) *J. Am. Chem. Soc.* **122**, 2142–2143
35. Schwieters, C. D., Kuszewski, J. J., Tjandra, N., and Clore, G. M. (2003) *J. Magn. Reson.* **160**, 65–73
36. Kuszewski, J., Gronenborn, A. M., and Clore, G. M. (1999) *J. Am. Chem. Soc.* **121**, 2337–2338
37. Grishaev, A., and Bax, A. (2004) *J. Am. Chem. Soc.* **126**, 7281–7292
38. Kuszewski, J. J., and Clore, G. M. (2000) *J. Magn. Reson.* **146**, 249–254
39. Rozhkova, A., Stirnimann, C. U., Frei, P., Grauschopf, U., Brunisholz, R., Grutter, M. G., Capitani, G., and Glockshuber, R. (2004) *EMBO J.* **23**, 1709–1719
40. Collet, J. F., Riemer, J., Bader, M. W., and Bardwell, J. C. A. (2002) *J. Biol. Chem.* **277**, 26886–26892
41. Aslund, F., Berndt, K. D., and Holmgren, A. (1997) *J. Biol. Chem.* **272**, 30780–30786
42. Quan, S., Schneider, L., Pan, J. L., Hacht, A. V., and Bardwell, J. C. (2007) *J. Biol. Chem.* **282**, 28823–28833
43. Pan, J. L., and Bardwell, J. C. A. (2006) *Protein Sci.* **15**, 2217–2227
44. Kim, J. H., Kim, S. J., Jeong, D. G., Son, J. H., and Ryu, S. E. (2003) *FEBS Lett.* **543**, 164–169
45. Grauschopf, U., Winther, J. R., Korber, P., Zander, T., Dallinger, P., and Bardwell, J. C. A. (1995) *Cell* **83**, 947–955
46. Krause, G., Lundstrom, J., Barea, J. L., Delacuesta, C. P., and Holmgren, A. (1991) *J. Biol. Chem.* **266**, 9494–9500
47. Segatori, L., Murphy, L., Arredondo, S., Kadokura, H., Gilbert, H., Beckwith, J., and Georgiou, G. (2006) *J. Biol. Chem.* **281**, 4911–4919
48. Zhao, Z., Peng, Y., Hao, S. F., Zeng, Z. H., and Wang, C. C. (2003) *J. Biol. Chem.* **278**, 43292–43298
49. Schmidt, B., Ho, L., and Hogg, P. J. (2006) *Biochemistry* **45**, 7429–7433
50. Qin, J., Clore, G. M., Kennedy, W. M., Huth, J. R., and Gronenborn, A. M. (1995) *Structure* **3**, 289–297
51. Qin, J., Clore, G. M., Kennedy, W. P., Kuszewski, J., and Gronenborn, A. M. (1996) *Structure* **4**, 613–620
52. Maeda, K., Hagglund, P., Finnie, C., Svensson, B., and Henriksen, A. (2006) *Structure* **14**, 1701–1710
53. Owens, R. A., and Hartman, P. E. (1986) *J. Bacteriol.* **168**, 109–114
54. Pittman, M. S., Corker, H., Wu, G. H., Binet, M. B., Moir, A. J. G., and Poole, R. K. (2002) *J. Biol. Chem.* **277**, 49841–49849
55. Pittman, M. S., Robinson, H. C., and Poole, R. K. (2005) *J. Biol. Chem.* **280**, 32254–32261
56. Fabianek, R. A., Hennecke, H., and Thony-Meyer, L. (2000) *FEMS Microbiol. Rev.* **24**, 303–316
57. Clamp, M., Cuff, J., Searle, S. M., and Barton, G. J. (2004) *Bioinformatics* **20**, 426–427

SUPPLEMENTAL DATA

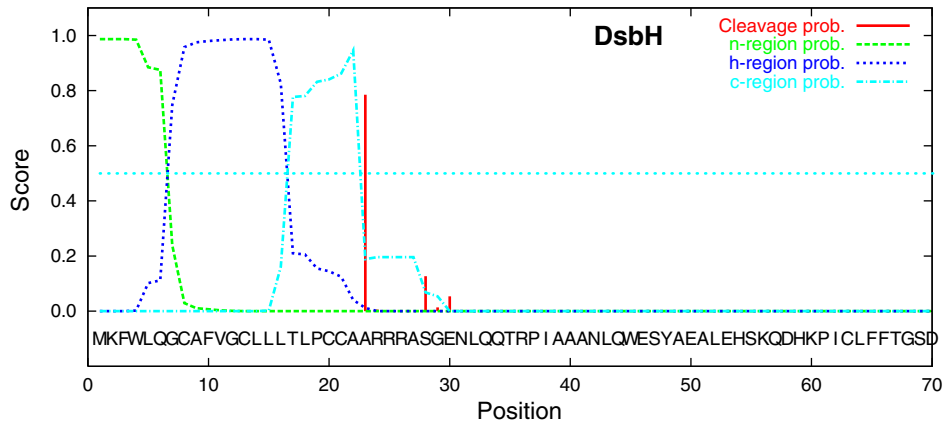
Insight into disulfide bond catalysis in *Chlamydia* from the structure and function of DsbH – a novel oxidoreductase

Thien-Thi Mac, Annekathrin von Hacht, Kuo-Chan Hung, Rachel J. Dutton, Dana Boyd, James C. A. Bardwell, and Tobias S. Ulmer

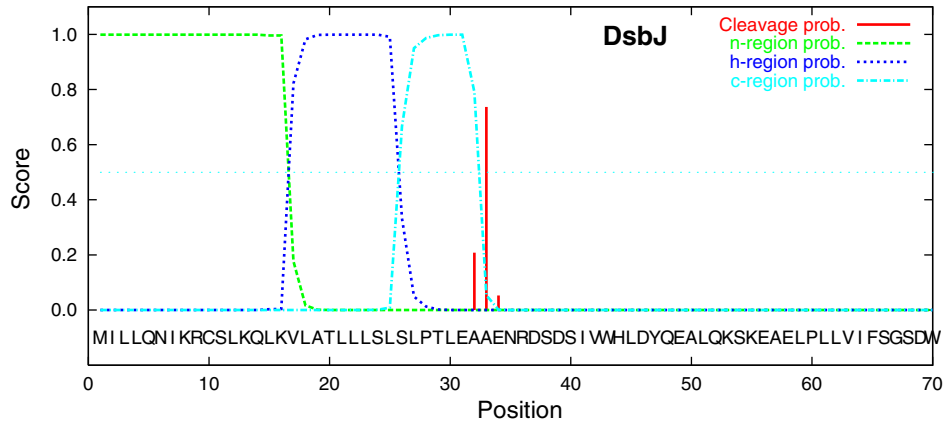
TABLE OF CONTENTS

Supplementary Figure 1. DsbH and DsbJ signal sequence prediction	S2
Supplementary Figure 2. Gel filtration of DsbH	S3
Supplementary Table 1. DsbH structural statistics	S4
Supplementary Table 2. Bacterial strains used	S5
Supplementary Table 3. Results spot titer for cadmium resistance	S6
Supplementary Table 4. Motility of the used strains in percent	S6
Supplementary Figure 3. Comparison of DsbH and DsbD γ active site geometries	S7

DsbH atomic coordinates, structural restraints and chemical shift assignments for DsbH have been deposited in the Protein Data Bank (<http://www.pdb.org>) and Biological Magnetic Resonance Bank (<http://www.bmrb.wisc.edu>) under ID codes 2ju5 and 15431, respectively.

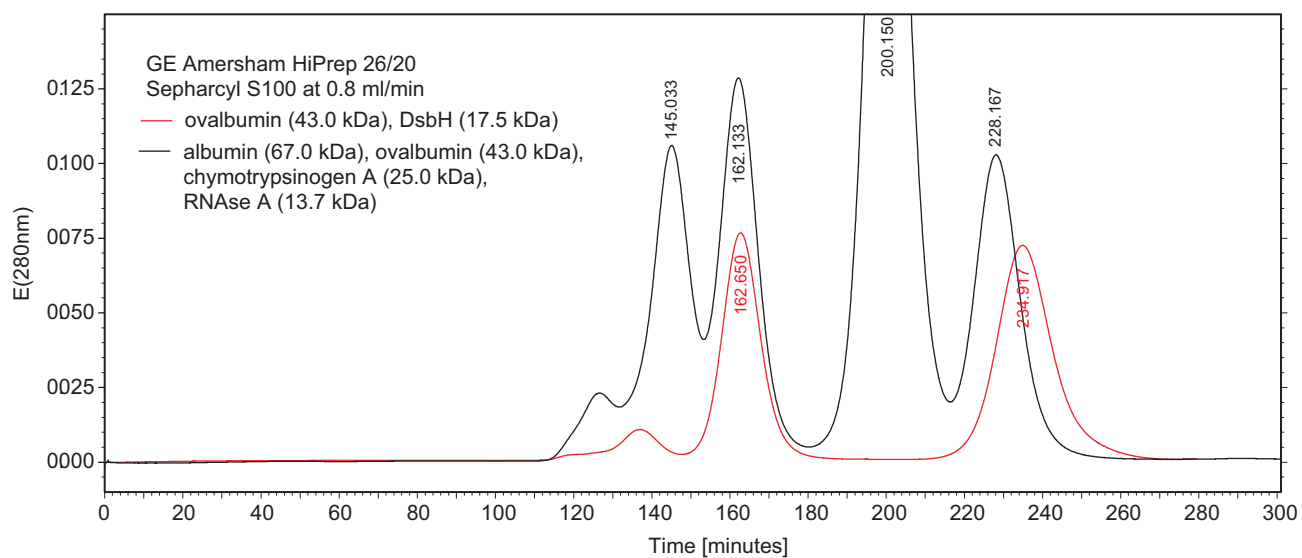


DsbH Signal peptide probability: 0.987
 Max cleavage site probability: 0.785 between pos. 22 and 23



DsbJ Signal peptide probability: 0.999
 Max cleavage site probability: 0.737 between pos. 32 and 33

Supplementary Figure 1. Hidden Markov models prediction (gram- models) of the signal sequences of DsbH and DsbJ using the program SignalP (Jannick Dyrlov Bendtsen, Henrik Nielsen, Gunnar von Heijne and Søren Brunak. J. Mol. Biol., 340:783-795, 2004). Within this model, the probabilities for DsbH and DsbJ to exhibit signal peptides are 0.987 and 0.999, respectively, clearly indicating their periplasmic localization. Other algorithms produce similar results.



Supplementary Figure 2. Gel filtration of DsbH (periplasmic) confirms its monomeric solution state. Ovalbumin was included in the run with DsbH to serve as internal reference.

Supplementary Table 1. DsbH structural statistics^a

R.m.s. deviations from experimental distance restraints (Å) ^b	
All (2479)	0.053 ± 0.001
Intraresidue (976)	0.029 ± 0.003
Interresidue sequential (i – j = 1) (644)	0.065 ± 0.002
Interresidue short range (1 < i – j < 5) (410)	0.063 ± 0.002
Interresidue long range (i – j ≥ 5) (449)	0.060 ± 0.003
R.m.s. deviations from experimental dihedral restraints (deg)	
All (257)	0.303 ± 0.041
R.m.s. deviations from experimental residual dipolar couplings (Hz) ^c	
¹ D _{NH} (bicelle) (114)	1.22 ± 0.03
¹ D _{NH} (gel) (115)	1.14 ± 0.03
¹ D _{CoC'} (bicelle) (111)	1.09 ± 0.02
¹ D _{CoC'} (gel) (110)	1.70 ± 0.03
¹ D _{NC'} (bicelle) (113)	1.07 ± 0.07
¹ D _{NC'} (gel) (111)	1.22 ± 0.07
Deviations from idealized covalent geometry	
Bonds (Å)	0.004 ± 0.0004
Angles (deg)	0.710 ± 0.010
Impropers (deg)	0.667 ± 0.015
Coordinate precision (Å) ^d	
Backbone nonhydrogen atoms	0.20 ± 0.05
All nonhydrogen atoms	0.69 ± 0.05
Measures of structural quality	
E _{LJ} (kcal mol ⁻¹) ^{3 e}	-632 ± 9
PROCHECK quality indicators	
Residues in most favorable region of Ramachandran plot ^f	89.5%
No. of bad contacts per 100 residues	2.8 ± 0.8

^a Statistics for the final 20 simulated annealing structures (residues 21-143).

^b None of the structures exhibited interproton distance violations greater than 0.52 Å or dihedral angle violations greater than 5°. Torsion angle restraints included 107 ϕ, 107 ψ, and 43 χ₁ angles.

^c R.m.s. deviations are normalized to an alignment tensor magnitude of 10 Hz. A normalized scalar product of -0.277 is obtained between the two alignment tensors.

^d Defined as the average r.m.s. difference between the final 20 simulated annealing structures and the mean coordinates (residues 21–143).

^e The Lennard–Jones van der Waals energy was calculated with the CHARMM PARAM 19/20 parameters and was not included in the simulated annealing target function.

^f There were no ϕ/ψ angles in the generously allowed or disallowed region of the Ramachandran plot.

Supplementary Table 2. Bacterial strains used

Strain or plasmid	Genotype or description	Reference/source
strain		
ER1821	<i>F glnV44 el4 mcrA⁻ rfb D1 relA1 endA1 spoT1 thi-1 Δ(mcrC-mrr)114::IS10</i>	New England Biolabs
IS13	JP120 pssTrx	Lab collection
IS394	JP120 pKK233-2	Lab collection
IS9	JP120 pssTrx-CPHC	Lab collection
JP373	ER1821 pKK233-2	Lab collection
JP120	ER1821 <i>dsbA::kan, zih12::Tn10</i>	Lab collection
BW25113	<i>rrnB3 ΔlacZ4787 hsdR514 Δ(araBAD)567 Δ(rhaBAD)568 rph-1</i>	Baba, T., T. Ara, M. Hasegawa, Y. Takai, Y. Okumura, M. Baba, K. A. Datsenko, M. Tomita, B. L. Wanner, and H. Mori. (2006) <i>Mol. Syst. Biol.</i> 2 (2006), p. 0008
BW25113 <i>dsbC::kan</i>	<i>rrnB3 ΔlacZ4787 hsdR514 Δ(araBAD)567 Δ(rhaBAD)568 rph-1 dsbC::kan</i>	Baba, T., T. Ara, M. Hasegawa, Y. Takai, Y. Okumura, M. Baba, K. A. Datsenko, M. Tomita, B. L. Wanner, and H. Mori. (2006) <i>Mol. Syst. Biol.</i> 2 (2006), p. 0008
BW25113 <i>dsbG::kan</i>	<i>rrnB3 ΔlacZ4787 hsdR514 Δ(araBAD)567 Δ(rhaBAD)568 rph-1 dsbG::kan</i>	Baba, T., T. Ara, M. Hasegawa, Y. Takai, Y. Okumura, M. Baba, K. A. Datsenko, M. Tomita, B. L. Wanner, and H. Mori. (2006) <i>Mol. Syst. Biol.</i> 2 (2006), p. 0008
SQ451	BL21, <i>dsbC::kan</i>	Lab collection
SQ453	BL21	Lab collection
plasmid		
pssTrx	pASK40-ss-trxA, thioredoxin exported via the DsbA signal sequence	Jonda, S., Huber-Wunderlich, M., Glockshuber, R., and Mossner, E. (1999) <i>Embo J.</i> 18 , 3271-3281
pKK233-2	cloning vector, pBR322 origin, Amp ^R	Pharmacia
pssTrx-CPHC	ssDsbA-trxA-CPHC in pKK233-2	lab collection

Supplementary Table 3. Results spot titer for cadmium resistance^a

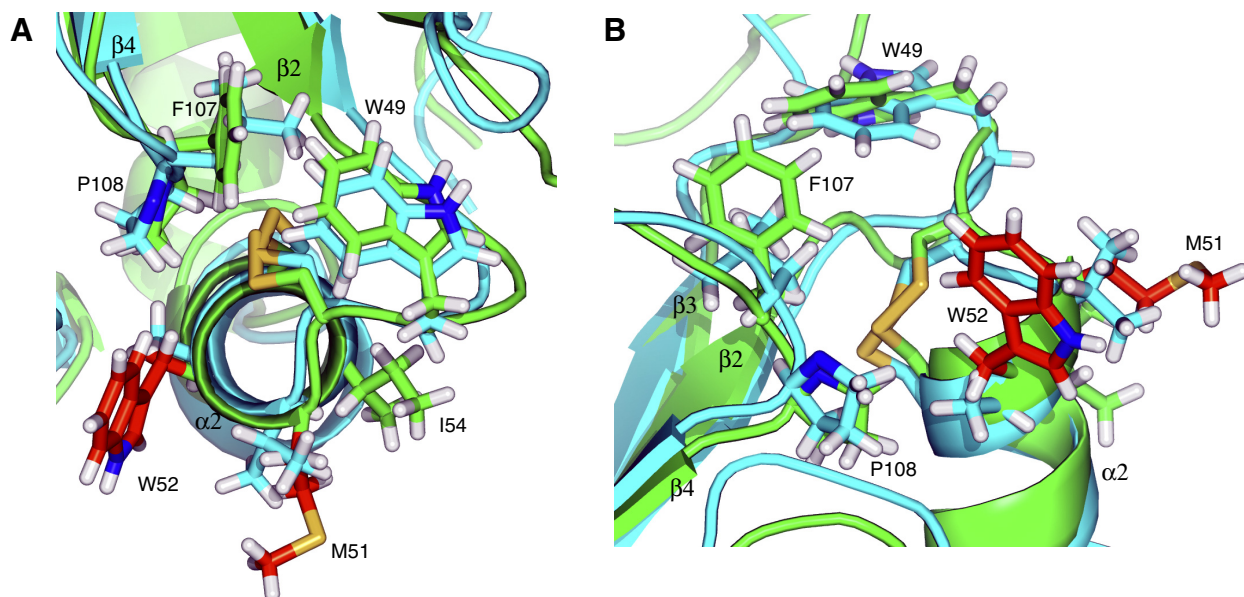
Strain	rank order
IS13	4
IS394	5
IS9	5
JP373	6
JP120	5
JP120 with pET44-DsbH	5

^a Cadmium resistance was ranked 1-7, with higher values indicating increased resistance.

Supplementary Table 4. Motility of the used strains in percent ^a

Strain	Motility (% of dsbA ⁺ strain)
JP120 DsbH	8.1
JP120	10
IS13	8.8
IS9	38.5
IS394	33.5
JP373	100

^a The motility of the dsbA⁺ strain (JP373) was set to 100%.



Supplementary Figure 3. Comparison of DsbH and DsbD γ active site geometries. **(A-B)**, Superposition of the active sites of DsbH (green) and E. coli DsbD γ (cyan; PDB entry 2FWE). Key amino acid residues are shown in ball-and-stick representation and are labeled for DsbH. K465 of DsbD γ is omitted for clarity.

Insight into Disulfide Bond Catalysis in *Chlamydia* from the Structure and Function of DsbH, a Novel Oxidoreductase

Thien-Thi Mac, Annekathrin von Hacht, Kuo-Chan Hung, Rachel J. Dutton, Dana Boyd, James C. A. Bardwell and Tobias S. Ulmer

J. Biol. Chem. 2008, 283:824-832.

doi: 10.1074/jbc.M707863200 originally published online November 14, 2007

Access the most updated version of this article at doi: [10.1074/jbc.M707863200](https://doi.org/10.1074/jbc.M707863200)

Alerts:

- [When this article is cited](#)
- [When a correction for this article is posted](#)

[Click here](#) to choose from all of JBC's e-mail alerts

Supplemental material:

<http://www.jbc.org/content/suppl/2007/11/15/M707863200.DC1>

This article cites 57 references, 23 of which can be accessed free at <http://www.jbc.org/content/283/2/824.full.html#ref-list-1>